

Supporting information of the manuscript
Supercritical hydrothermal synthesis of UO_{2+x} :
Stoichiometry, crystal shape and size, and homogeneity
observed using ^{23}Na -NMR spectroscopy of $(\text{U},\text{Na})\text{O}_{2+x}$

October 21, 2021

1 Effects of additives on morphologies of UO_2 particles

The aspect ratios of the obtained particles, which we define as the statistical ratio of the particle dimensions (long to small axes), were evaluated using scanning electron microscopy images. Figure 1 shows the histograms of the aspect ratios of the UO_2 samples using combinations of ethanol and various additives.

Figure 2 shows the histograms of the aspect ratios of the UO_2 samples prepared using the additives methanol, 2-propanol, ammonium carbonate (AC), and propionaldehyde (PA).

Figure 3 shows the histograms of the aspect ratios of the UO_2 samples prepared using the additives hexylamine and hexylaldehyde.

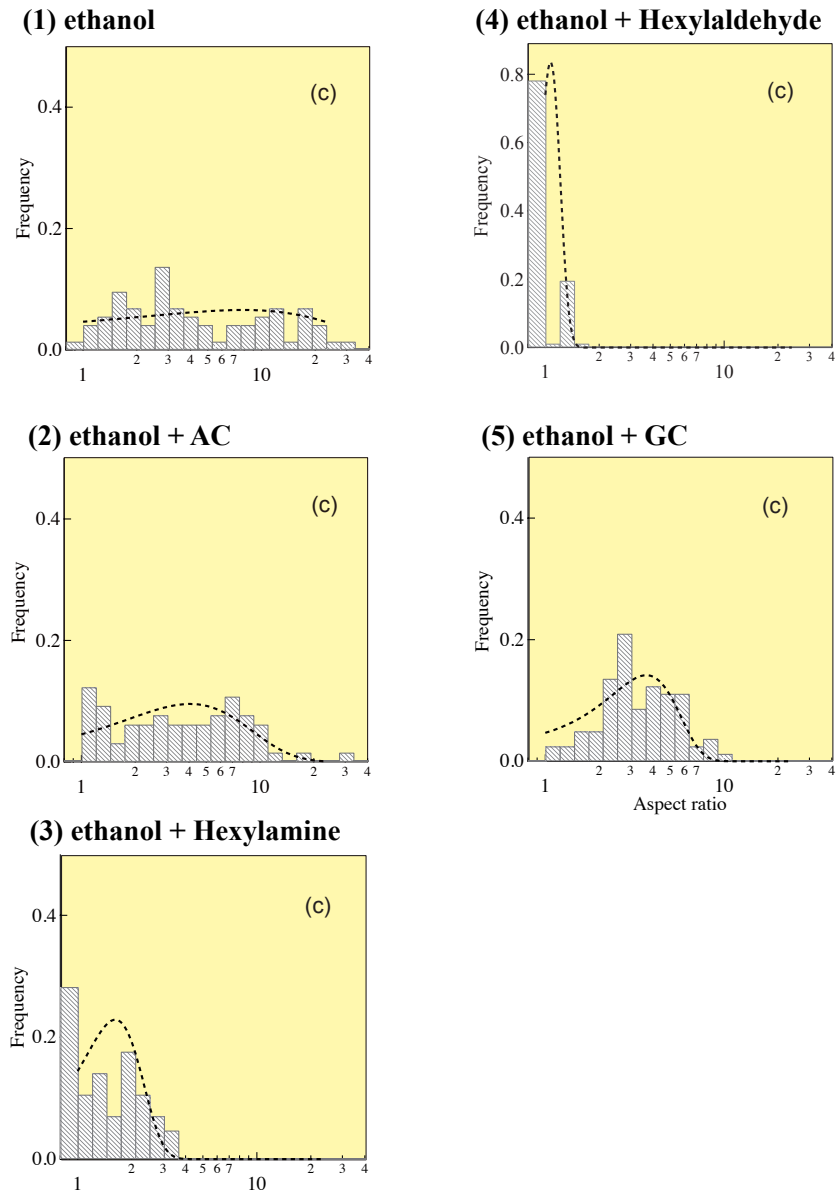


Figure 1: Aspect ratios (statistical ratio of particle dimensions of long to small axes) of the particle sizes of the UO_2 samples prepared with the addition of (1) ethanol (Sample 3-1-1), (2) ethanol and ammonium carbonate (AC, Sample 3-1-2), (3) ethanol and hexylamine (Sample 3-1-3), (4) ethanol and hexylaldehyde (Sample 3-1-4), and (5) ethanol and guanidine carbonate (GC, Sample 3-1-5).

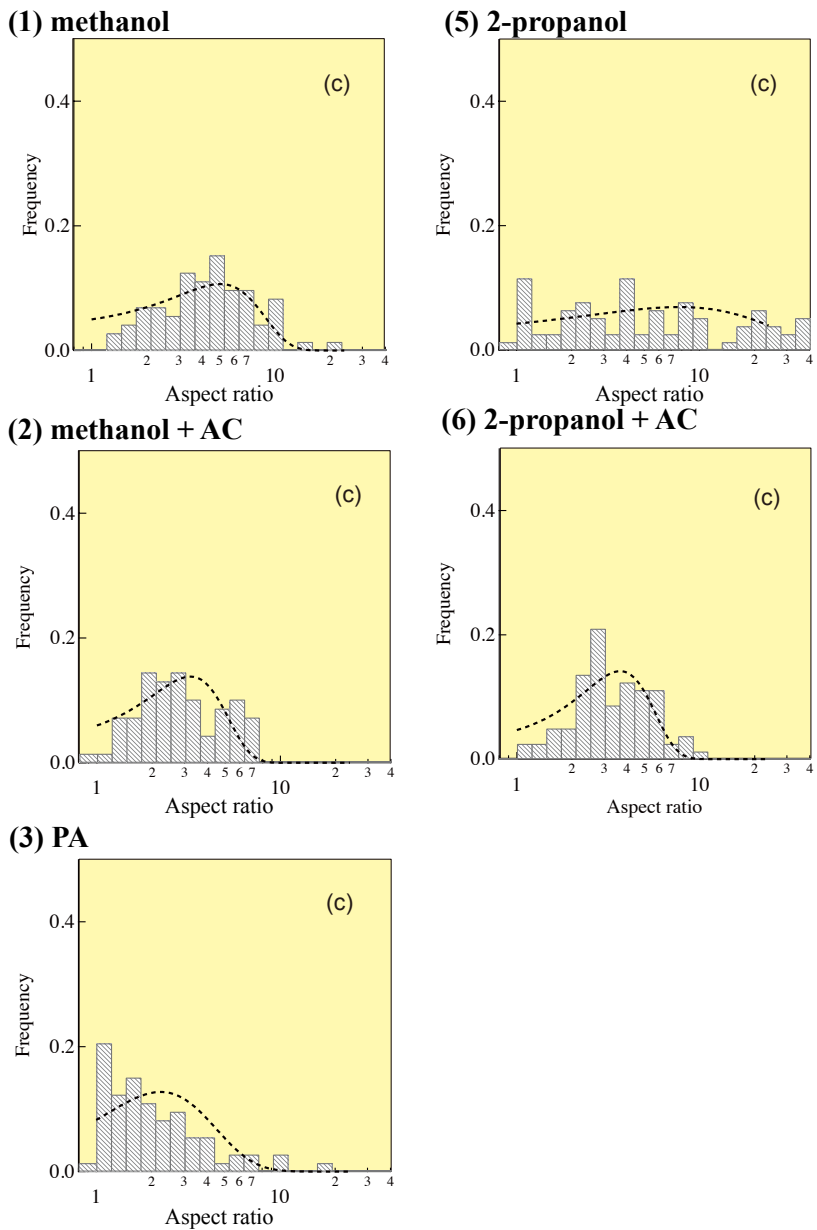
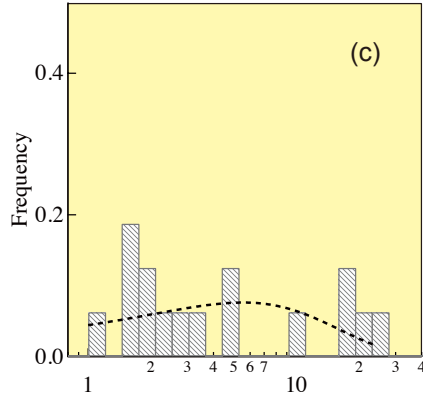


Figure 2: Figure 2: Aspect ratios (statistical ratio of particle dimensions of long to small axes) of the particle sizes of the UO_2 samples prepared with the addition of (1) methanol (Sample 3-2-1), (2) methanol and ammonium carbonate (AC, Sample 3-2-2), (3) propionaldehyde (PA, Sample 3-3-1), (5) 2-propanol (Sample 3-4-1), and (6) 2-propanol and AC (Sample 3-4-2). Aspect ratios for (4) PA and AC (Sample 3-3-2) are not displayed because these are spherical particles.

(1) Hexylamine



(2) Hexylaldehyde

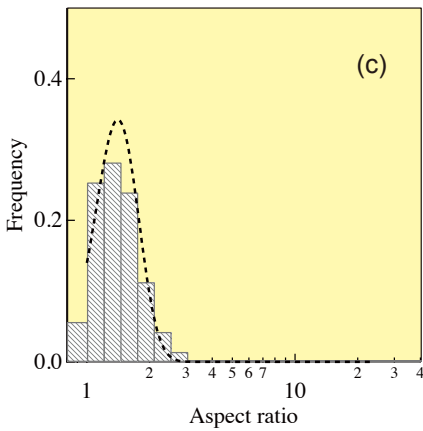


Figure 3: Figure 3: Aspect ratios (statistical ratio of particle dimensions of long to small axes) of the particle sizes of the UO_2 samples prepared with the addition of (1) hexylamine (Sample 3-5-1) and (2) hexylaldehyde (Sample 3-5-2).

2 Sample characterization of $(\text{U}, \text{Na})_{2+x}$ using X-ray diffraction (XRD)

Figure 4 shows X-ray diffraction patterns of $(\text{U}, \text{Na})\text{O}_{2+x}$ samples prepared using hydrothermal synthesis. All the observed diffraction peaks are assigned to the Bragg reflections of the fluorite structure (space group: $\text{Fm}\bar{3}\text{m}$), with no impurity peak.

3 Rietveld analyses of XRD patterns

The diffractogram of the typical result of the Rietveld analysis using RIETAN-FP [1] is shown in Fig. 5.

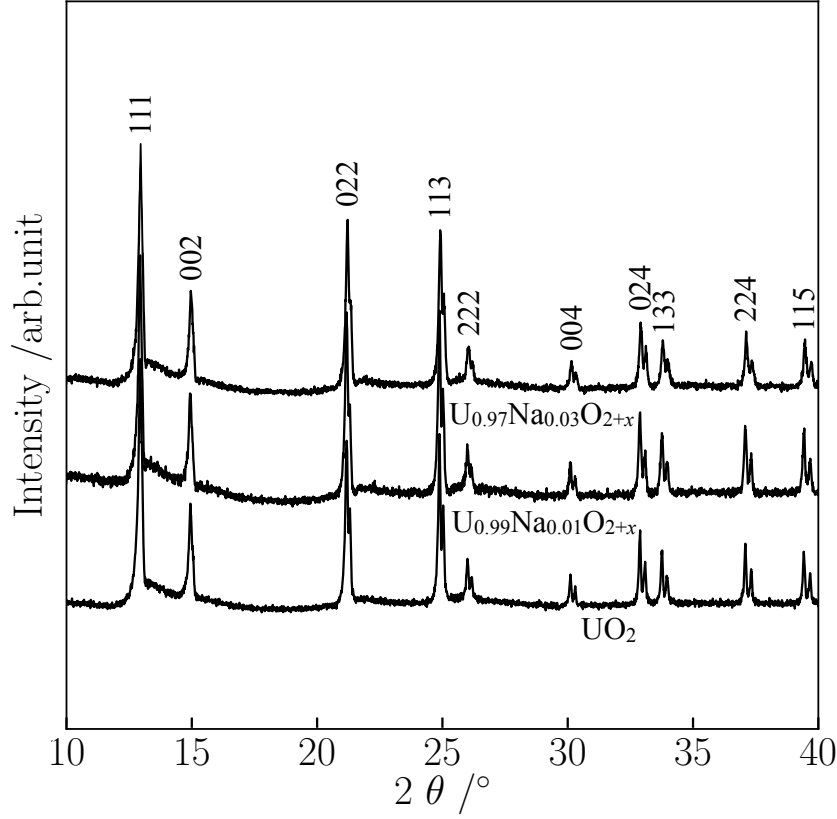


Figure 4: XRD diffraction patterns of the prepared samples of UO_{2+x} (Sample 4-1), $\text{U}_{0.99}\text{Na}_{0.01}\text{O}_{2+x}$ (Sample 4-2), and $\text{U}_{0.97}\text{Na}_{0.03}\text{O}_{2+x}$ (Sample 4-3).

4 ^{23}Na -NMR spectroscopy of $(\text{U},\text{Na})\text{O}_2$

Figure 6 shows a typical example of the experiment performed on a Na 3% substituted sample to determine the ^{23}Na -NMR signal, which is observed near the ^{63}Cu -NMR signal of the Cu wire (Fig. 6). This signal is due to Na and Cu, which is confirmed by the absence of any peak near the ^{65}Cu -NMR signal (Fig. 6).

Based on the position of the peaks in the NMR spectrum, the Knight shift K can be evaluated, using the relationship of

$$K \equiv \frac{H_0 - H_{\text{res}}}{H_{\text{res}}} = \frac{2\pi\nu_L - \gamma_n H_{\text{res}}}{\gamma_n H_{\text{res}}}, \quad (1)$$

where H_{res} , ν_L , γ_n are the shifted peak position, the constant frequency, and gyromagnetic ratio, respectively. Figure 7 shows the temperature dependence of the Knight shift. Below the antiferromagnetic transition temperature of $T_N \sim 30$ K, the peak became a broad powder pattern typically observed in antiferromagnets. The Knight shift below T_N was determined by the frequencies at both sides of the broadened peak in the spectrum.

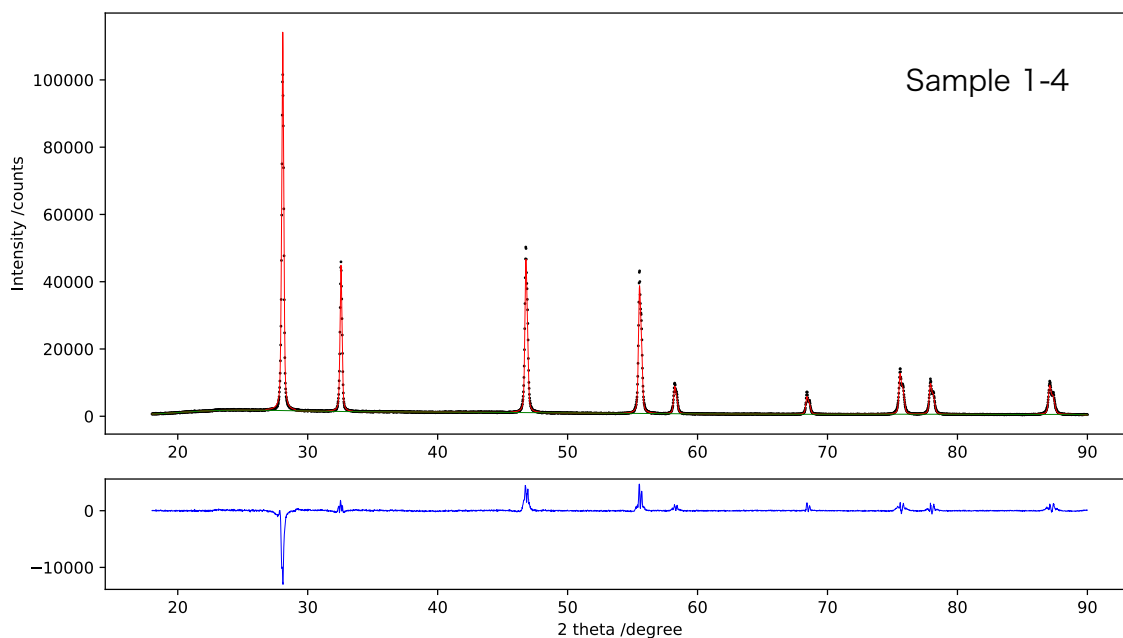


Figure 5: Diffractogram of a typical Rietveld analysis result (Sample 1-4).

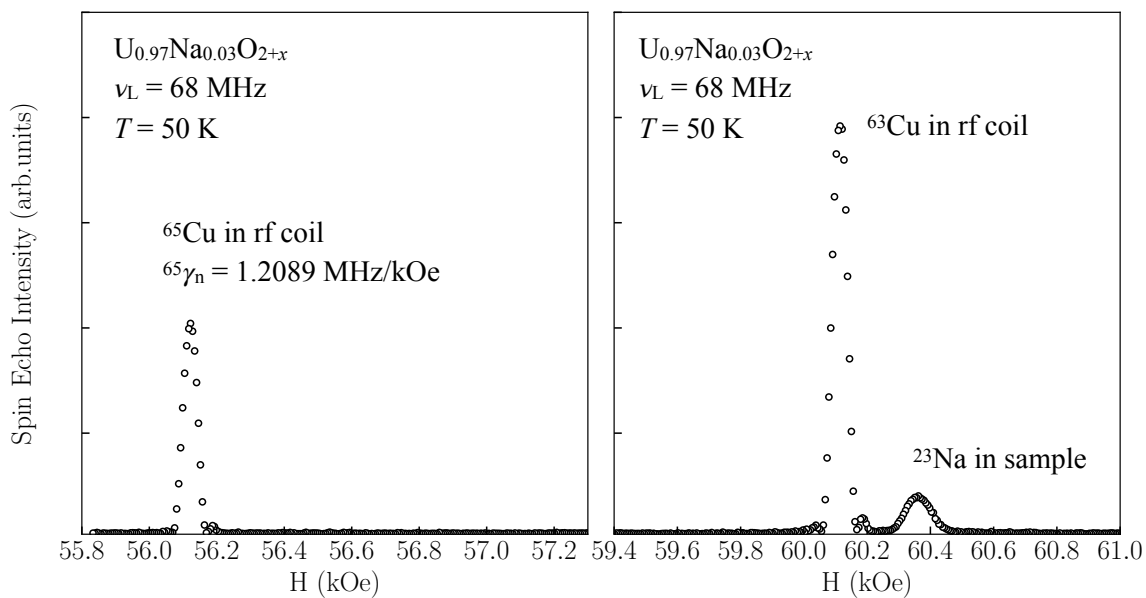


Figure 6: Magnetic field-swept NMR spectra of the standard sample $U_{0.97}Na_{0.03}O_{2+x}$, (Left panel) near ^{65}Cu NMR signal and (Right panel) near ^{65}Cu NMR signal from the rf coil.

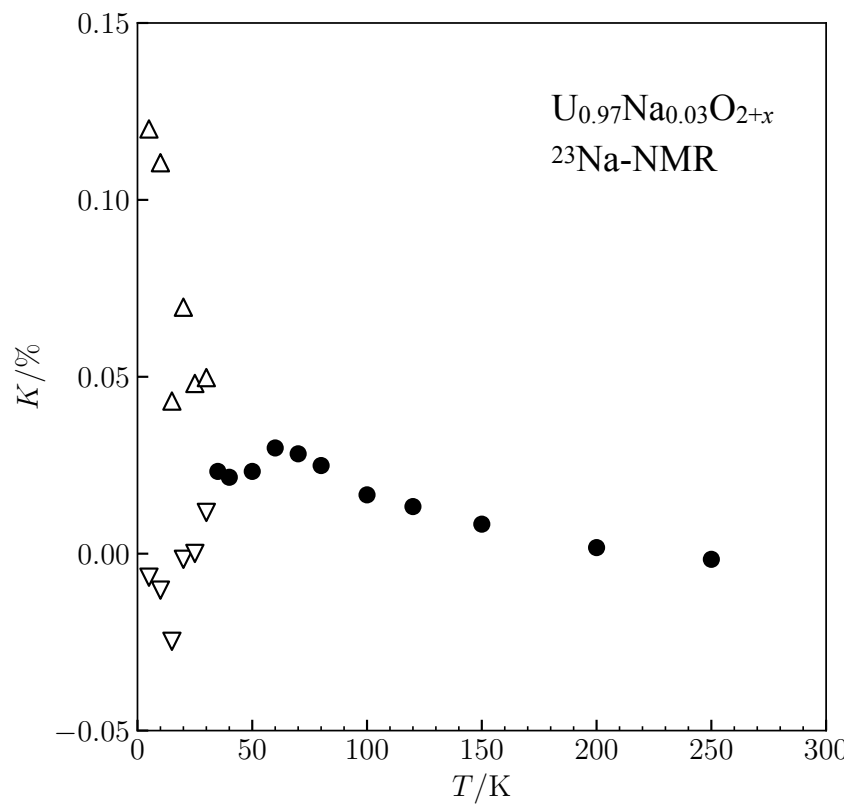


Figure 7: Temperature dependence of the Knight shift of the $(U, Na)O_2$.

References

- [1] Izumi, F.; Momma, K. *Solid State Phenom.* **2007**, *130*, 15–20.